

## Shape Reconstruction with A Priori Knowledge Based on Integral Invariants\*

Thomas Fidler<sup>†</sup>, Markus Grasmair<sup>†</sup>, and Otmar Scherzer<sup>‡</sup>

**Abstract.** We investigate the applicability of integral invariants as geometrical shape descriptors in the context of ill-posed inverse problems. We propose the use of a Tikhonov functional, where the penalty term is based on the difference of integral invariants. As a case example, we consider the problem of inverting the Radon transform of an object with only limited angular data available. We approximate the ill-posed operator equation by a minimization problem involving a Tikhonov functional and show existence of minimizers of the functional. Because of its nondifferentiability, we derive for the numerical minimization smooth approximations, which converge in the sense of  $\Gamma$ -limits.

**Key words.** inverse problems, Radon transform, integral invariants, Tikhonov regularization,  $\Gamma$ -convergence, shape invariants, shape optimization

**AMS subject classifications.** 65J15, 65J20, 49J45

**DOI.** 10.1137/110824735

**1. Introduction.** A typical task in object recognition is to segment an object in an image. In some cases, however, the image is not directly accessible, but only a transformed version of the image, e.g., its Radon transform, which may occur if the object is inspected with a tomograph. Then the information of interest—the objects within the image—has to be reconstructed from the given data set. In mathematical terms, this task can be formulated as the inverse problem of solving an operator equation of the form

$$F[\Omega] = y,$$

where  $F$  describes the image formation process, i.e., the action of the tomograph on the object  $\Omega$ , and  $y$  denotes the available data.

The previous operator equation is a typical example of an ill-posed problem: the solution does not depend continuously on the data  $y$ . In addition, to ensure that biological harm caused by the radiation is reduced to a minimum, it might be advisable to perform the scan only for a limited number of directions. Then, it is well known from mathematical theory that the recorded data is insufficient for a unique reconstruction of the object, unless ample prior information is available. In order to stabilize the reconstruction process, it is therefore necessary to introduce some kind of regularization. One common approach is to

\*Received by the editors February 15, 2011; accepted for publication (in revised form) March 6, 2012; published electronically June 28, 2012. This work was supported by the Austrian Science Fund (FWF) within the national research networks *Industrial Geometry*, project S9203-N12, and *Photoacoustic Imaging in Biology and Medicine*, project S10505-N20.

<http://www.siam.org/journals/siims/5-2/82473.html>

<sup>†</sup>Computational Science Center, University of Vienna, 1090 Vienna, Austria ([thomas.fidler@univie.ac.at](mailto:thomas.fidler@univie.ac.at), [markus.grasmair@univie.ac.at](mailto:markus.grasmair@univie.ac.at)).

<sup>‡</sup>Computational Science Center, University of Vienna, 1090 Vienna, Austria, and Radon Institute of Computational and Applied Mathematics, 4040 Linz, Austria ([otmar.scherzer@univie.ac.at](mailto:otmar.scherzer@univie.ac.at)).

use an iterative method for the solution of the equation but to stop the iteration well before the onset of convergence. In this case it is very easy to incorporate a priori knowledge in terms of closeness to some prior by choosing the starting point of the iteration. This method of selecting the correct solution is also supported by the mathematical theory of iterative regularization methods. A different method is the reformulation of the operator equation as a functional with a fit-to-data term and a regularization term. The fit-to-data term ensures that the solution closely matches the given data, and the additionally introduced regularization term incorporates some knowledge about the solution while at the same time enforcing well-posedness.

Often, the a priori knowledge can be formulated as a regularity constraint on the solution. As an example, for segmenting an object in a given image, often a Tikhonov-like functional is used, where the squared norm of the gradient of the boundary curve ensures the regularity of the object to be segmented. In the field of shape recovery, additionally, the a priori information may often include geometrical information about the object. Thus the regularization term has to be constructed in such a way that the geometry of the solution is close to the geometry of the prior.

At this point, naturally, the question arises of how to describe the geometry of an object in a mathematical terminology. A classical approach uses the curvature of the boundary curve of the object to define feature points, as geometrical features like protrusions, corners, or inflection points can all be characterized by their curvature. All invariants, however, that are based on differentiation—thus, in particular, curvature—suffer from an inherent sensitivity regarding noise. As a remedy, it has been suggested to replace differentiation by integration in such a way that the ensuing *integral invariants* still carry geometrical information about the object [5, 19, 20, 22]. These invariants have proven to be successful for object classification [19] and geometry processing [14].

This article intends to show that integral invariants can also be used for the solution of inverse problems in the context of shape recovery. To that end we propose using a penalty term which includes the  $L^2$ -norm of the difference between the invariant of the object and the invariant of a prior. Since this penalty term is geometry based, it is expected that this procedure will yield more accurate reconstructions than simpler methods based on a metric between the objects themselves, e.g., the area of the set symmetric difference or the Hausdorff distance. Indeed, the performed numerical study, which uses the Radon transform as a paradigm of an inverse problem, supports these expectations. To highlight the applicability of our method to severely ill-posed problems, we limited the number of directions in which the Radon transform was computed to four, leading to a high number of possible solutions. Note, however, that we try to reconstruct only shapes, that is, binary distribution functions, and not arbitrary ones. The possibility of reconstructing such data in the presence of sufficient a priori knowledge has been demonstrated in [24]; there a level set method has been used for the regularization.

In section 2 we briefly recall the notion of shapes and introduce the concept of integral invariants as robust geometry-based shape descriptors. Section 3 is devoted to the theoretical background of inverting the Radon transform of an object. First we introduce the problem in a strict mathematical manner, which also includes a reformulation of the problem originally posed on a class of objects as a nonlinear operator equation on a Hilbert space. The resulting

operator being nondifferentiable, we derive a smooth approximation, which is later used in the numerical implementation. In section 4, we perform a case study using synthetic data and compare the proposed method with a Landweber–Kaczmarz method using the prior as an initial guess. Both approaches turn out to be capable of reconstructing the rough shape of the object, but the Landweber–Kaczmarz method introduces artificial perturbations of the object’s boundary, whereas Tikhonov regularization with integral invariants does not.

**2. Regularization with integral invariants.** Suppose we have an operator  $F: X \rightarrow Y$ , which maps a shape  $x$  to some given data  $y$ , i.e.,

$$(2.1) \quad F[x] = y.$$

We assume that the data set  $y$  is available through some measurement setup and the underlying physical principle is described by the operator  $F$ . We focus on the inverse problem of finding a suitable shape  $x$  matching the data  $y$ . The first question arising at this point is the well-posedness of the problem. The failure of well-posedness may be due to various reasons, e.g., discontinuity of the inverse operator. In this article we mainly consider one specific type of ill-posedness in the area of inverse problems: multiple solutions because of incomplete or insufficient data.

Assuming that the available data  $y$  is insufficient for solving (2.1) uniquely, we have to regularize the original operator equation. In shape optimization and reconstruction a common approach to stabilizing the process of solving (2.1) is to use a prior incorporating some knowledge of the solution. The prior can be seen as a reference model that covers the essential information about the object. A typical choice is some representative of the shape, generated from a set of training data using statistical methods. In that context the possible variations of the shapes are explained in terms of statistics, e.g., using a principal component analysis where the shapes are points on a possible infinite-dimensional manifold [6, 8, 25] (see also [21]). In contrast, we propose using integral invariants to explain and handle the variability of a shape. This concept has been applied successfully to segmentation with priors [20] but not yet for more general inverse and ill-posed problems.

In the following we briefly introduce the concept of shapes and integral invariants.

**2.1. Shapes.** We consider a shape as a characteristic function of a given simply connected and bounded set  $\Omega \subset \mathbb{R}^2$ . In addition, we restrict ourselves to objects that are star-shaped with respect to the origin and therefore can be represented by a nonnegative radial function.

**Definition 2.1.** Let  $\gamma \in L^2(\mathbb{S}^1, \mathbb{R}_+) := \{\gamma \in L^2(\mathbb{S}^1, \mathbb{R}) : \gamma \geq 0\}$ . The set

$$(2.2) \quad \Omega_\gamma := \{t\tau \in \mathbb{R}^2 : \tau \in \mathbb{S}^1, 0 \leq t \leq \gamma(\tau)\}$$

is called the domain generated by the nonnegative radial function  $\gamma$ .

Notice that the assumption  $\gamma \in L^2(\mathbb{S}^1, \mathbb{R}_+)$  is necessary (and sufficient) to guarantee that the object  $\Omega_\gamma$  has a finite area. Indeed, a short calculation reveals that

$$\mathcal{L}^2(\Omega_\gamma) = \frac{1}{2} \int_{\mathbb{S}^1} \gamma^2(\tau) d\mathcal{H}^1(\tau) = \frac{1}{2} \|\gamma\|_{L^2}^2 < \infty,$$

where  $\mathcal{L}^2$  and  $\mathcal{H}^1$  denote the Lebesgue and the Hausdorff measure, respectively.

An intuitive definition of shapes was given by Kendall [17, p. 2]: a shape is “*what is left when the differences which can be attributed to translations, rotations, and dilatations have been quotiented out.*” In contrast, by our definition the shape changes if one applies a rigid body motion. Hence, it would be more common to use the notion of objects rather than that of shapes. But at least we have retained some invariance with respect to rotations (cf. Definition 2.2): a rotation of  $\Omega_\gamma$  simply corresponds to a shift of the argument of the radial function  $\gamma$ .

**2.2. Integral invariants.** We now briefly recall the concept of integral invariants and introduce the circular integral invariant, which has proven to be useful in applications. A reader interested in this topic may find useful background information in the articles of Manay et al. [19] or in [4, 5].

The basic idea of integral invariants is closely related to that of differential invariants but with an emphasis on stability with respect to noise. In contrast to differential invariants (cf. [2]), which are based on derivatives, the key to noise insensitivity of integral invariants is the replacement of differentiation by integration. Apart from that, the main features of differential invariants should be retained, e.g., a possible geometrical interpretation or invariance with respect to some group operation. In case of the curvature of the boundary curve of a sufficiently regular object—the most common representative of differential invariants—we have an obvious geometrical interpretation and also invariance with respect to rigid body motions. More precisely, invariance holds if it is understood in the following sense.

**Definition 2.2.** A mapping  $I: L^2(\mathbb{S}^1, \mathbb{R}_+) \rightarrow L^1(\mathbb{S}^1, \mathbb{R}_+)$  is invariant with respect to the group of rotations  $SO(2)$  if

$$(2.3) \quad I[\gamma](\tau) = I[\gamma \circ h](h\tau) \quad \text{for all } h \in SO(2).$$

In [22] it has been shown that the area of the intersection of an object with a ball centered at its boundary is closely related to the curvature of the boundary of the object. This provides a motivation for the following definition of the circular integral invariant first introduced by Manay et al. [19].

**Definition 2.3.** Let  $R > 0$ , and define  $B_R(x) := \{y \in \mathbb{R}^2 : \|x - y\|_2 < R\}$ . The operator  $\mathcal{I}_R: L^2(\mathbb{S}^1, \mathbb{R}_+) \rightarrow L^1(\mathbb{S}^1, \mathbb{R}_+)$  defined by

$$(2.4) \quad \mathcal{I}_R[\gamma](\tau) := \mathcal{L}^2\left(\Omega_\gamma \cap B_R(\gamma(\tau)\tau)\right),$$

where  $\Omega_\gamma$  denotes the domain generated by the radial function  $\gamma$  (see Definition 2.1), is called the circular integral invariant (cf. Figure 1).

**Theorem 2.4.** The circular integral invariant of Definition 2.3 is continuous.

*Proof.* Assume that  $\gamma_k$  converges to  $\gamma$  in  $L^2(\mathbb{S}^1, \mathbb{R}_+)$ . Then we obtain for almost every  $\tau \in \mathbb{S}^1$  that  $\gamma_k(\tau) \rightarrow \gamma(\tau)$ . As a consequence, we see that for almost every  $\tau \in \mathbb{S}^1$  we have that  $\chi_{B_R(\gamma_k(\tau)\tau)} \rightarrow \chi_{B_R(\gamma(\tau)\tau)}$  pointwise almost everywhere. In addition, we know that  $\chi_{\Omega_{\gamma_k}}$  converges pointwise almost everywhere to  $\chi_{\Omega_\gamma}$  and, consequently, for almost every  $\tau \in \mathbb{S}^1$ ,

$$\chi_{\Omega_{\gamma_k}} \chi_{B_R(\gamma_k(\tau)\tau)} \rightarrow \chi_{\Omega_\gamma} \chi_{B_R(\gamma(\tau)\tau)} \quad \text{pointwise almost everywhere.}$$

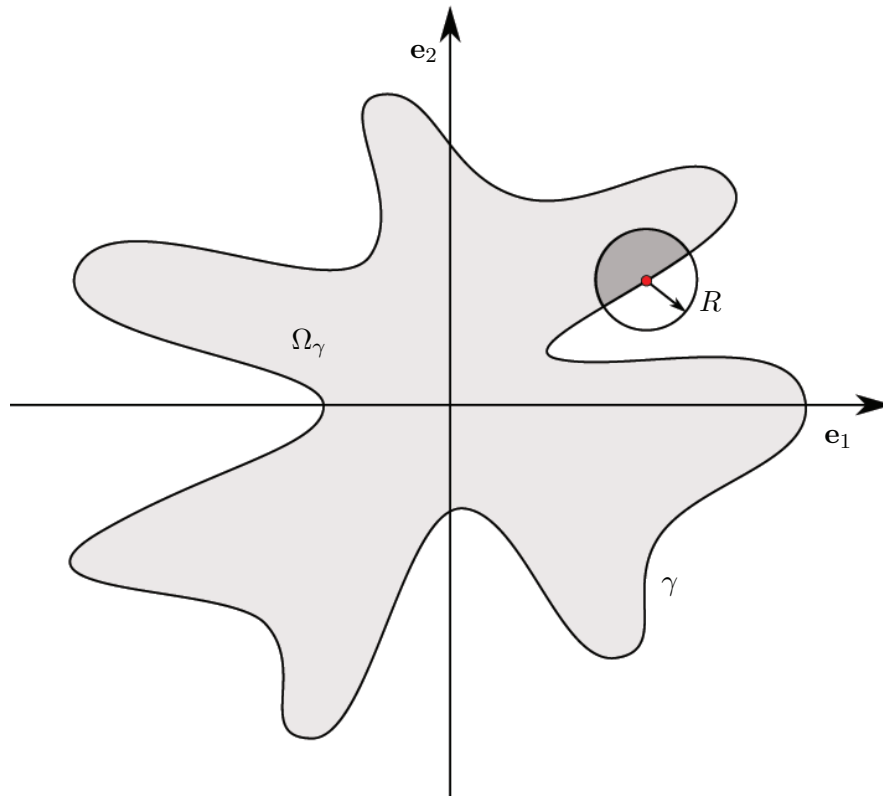


Figure 1. Visualization of the definition of the circular integral invariant.

Applying Lebesgue's theorem of dominated convergence twice, we see that

$$\begin{aligned} & \int_{\mathbb{S}^1} |\mathcal{I}_R[\gamma](\tau) - \mathcal{I}_R[\gamma_k](\tau)| d\mathcal{H}^1(\tau) \\ &= \int_{\mathbb{S}^1} \left| \int_{\mathbb{R}^2} \chi_{\Omega_\gamma \cap B_R(\gamma(\tau)\tau)}(x) d\mathcal{L}^2(x) - \int_{\mathbb{R}^2} \chi_{\Omega_{\gamma_k} \cap B_R(\gamma_k(\tau)\tau)}(x) d\mathcal{L}^2(x) \right| d\mathcal{H}^1(\tau) \rightarrow 0, \end{aligned}$$

which concludes the proof. ■

It is worth pointing out that the circular integral invariant is a stable approximation of the curvature of the object's boundary curve in the limit as  $R$  tends to 0. As a consequence, regions of high curvature—commonly seen as features of the object—are mapped to features of the corresponding circular integral invariant, allowing for direct identification. More precisely, one obtains the relation

$$\mathcal{I}_R[\gamma](\tau) = \frac{\pi}{2}R^2 - \frac{\kappa_\gamma(\tau)}{3}R^3 + O(R^4)$$

with  $\kappa_\gamma(\tau)$  denoting the curvature of  $\gamma$  at the point  $\gamma(\tau)$  (see [15, 22]). While it is well known that the curvature function of a sufficiently regular arc length parametrized curve encodes the underlying object uniquely up to rigid body motions, so far the uniqueness for the circular integral invariant for fixed  $R > 0$  is still an open question. Note, however, that a result

towards this aim has recently been derived in [1], which shows local uniqueness for curves  $\gamma$  that are sufficiently close to a circle.

A more detailed discussion of the circular integral invariant is presented in [5]. In addition, one can find there an explicit formula in terms of the radial function (cf. [5, Lemma 4.2]). The same formula is used for the implementation of the invariant in the numerical examples below. Also, the Radon transform of a star-shaped object, the stable approximate inversion of which is considered in our case example, is rewritten in terms of the radial function. This enables us to work within the functional analytic setting of the Hilbert space  $L^2(\mathbb{S}^1, \mathbb{R})$ .

*Remark 2.5.* Given a star-shaped object in the plane, there are many different possibilities for describing it in terms of a radial function, depending on the choice of the center of star-shapedness and the orientation of the object. Concerning the choice of the center of star-shapedness, it can be shown that the set of all centers of a star-shaped object is convex and therefore admits a unique center of mass that is again a center of star-shapedness. The situation is more complicated for the orientation of the object. Here, one can, for instance, align the object such that the mean direction of the radial function equals the first standard basis vector of  $\mathbb{R}^2$ . This alignment, however, is only possible if a mean direction exists, which need not be the case in the presence of symmetries within the object.

**3. Example: Shape reconstruction based on the Radon transform.** In this section we consider the problem of reconstructing an object from a given data set that represents the Radon transform of the object in some predefined directions. More mathematically, this task can be formulated as an inverse problem as follows: Find an object  $\Omega$  such that its Radon transform  $\mathbf{R}_{\sigma_i}$  for finitely many given directions  $\sigma_i$ ,  $i = 1, \dots, n$ , matches the data  $y_i$ . In other words, find a solution of

$$(3.1) \quad \mathbf{R}_{\sigma_i}[\Omega] = y_i, \quad i = 1, \dots, n.$$

Since we are given only finitely many directions, the problem of solving (3.1) is ill-posed, and therefore we have to apply some regularization incorporating a priori information about the geometry of the objects to be reconstructed. In the following we show how information based on integral invariants can be used in a Tikhonov-like regularization method on the set of all nonnegative radial functions generating star-shaped objects. In particular, we end up with a shape optimization problem, where the admissible shapes are restricted to those that can be represented by a nonnegative radial function. Similar inverse problems for star-shaped objects have been considered by Hettlich and Rundell (cf. [10, 11, 12]) using different approaches to stabilize the inversion, among them iterative schemes and also Tikhonov regularization. In contrast to their proposed methods including only smoothness assumptions, we explicitly incorporate additional geometric information by means of the circular integral invariant.

*Remark 3.1.* In practical applications, it is unrealistic to assume that the considered objects (and also their background) are truly homogeneous. Instead of being constant, the absorption coefficient in the object can be expected to vary slightly around some mean. If these variations are sufficiently small and unstructured, then they can be treated in the same way as measurement errors; if an appropriate regularization method is used, then the proposed model therefore still allows for an acceptable reconstruction. See also the argumentation

in [24], where a similar model has been used successfully for the direct estimation of interfaces from sparse tomographic data.

**3.1. The optimization problem.** We now reformulate the geometrical definition of the standard Radon transform in terms of the generating radial function. For that purpose we introduce an operator  $\mathcal{R}_{\sigma_i}$  that first maps the radial function  $\gamma$  to the object it generates and afterwards applies to this object the standard Radon transform restricted to a specific direction  $\sigma_i \in \mathbb{S}^1$ . As mentioned in Remark 2.5, it would be necessary to introduce two additional parameters into the optimization problem, the center of star-shapedness and the orientation of the object. For simplicity we neglect these parameters in the considerations below, but refer to Remark 4.1 at the end of section 4, where some ideas are presented on how they can be incorporated into applications.

**Definition 3.2.** Let  $\sigma_i \in \mathbb{S}^1$ , and define the operator  $\mathcal{R}_{\sigma_i}: L^2(\mathbb{S}^1, \mathbb{R}_+) \rightarrow L^1(\mathbb{R}, \mathbb{R})$  by

$$(3.2) \quad \mathcal{R}_{\sigma_i}[\gamma](\alpha) := \int_{\mathbb{R}} \chi_{\Omega_\gamma}(\alpha \sigma_i^\perp + t \sigma_i) d\mathcal{L}^1(t).$$

Notice that the geometrical interpretation of  $\mathcal{R}_{\sigma_i}[\gamma]$  and the standard Radon transform of  $\Omega_\gamma$  coincide. The major difference is the nonlinearity of  $\mathcal{R}_{\sigma_i}$  with respect to the radial function  $\gamma$ .

**Lemma 3.3.** The operator  $\mathcal{R}_{\sigma_i}$  of Definition 3.2 is continuous.

We now define the Tikhonov regularization of (3.1) in a precise mathematical manner.

**Definition 3.4.** Let  $\beta, \mu > 0$  and  $\gamma_{\text{ref}} \in L^2(\mathbb{S}^1, \mathbb{R}_+)$ . In addition, denote by  $\mathcal{I}: L^2(\mathbb{S}^1, \mathbb{R}_+) \rightarrow L^1(\mathbb{S}^1, \mathbb{R}_+)$  the circular integral invariant defined by (2.4). For  $\sigma_i \in \mathbb{S}^1$  and  $f_i \in L^2(\mathbb{R}, \mathbb{R})$ ,  $i = 1, \dots, n$ , define

$$\mathcal{D}_{\sigma_i}[\gamma] := \frac{1}{2} \|\mathcal{R}_{\sigma_i}[\gamma] - f_i\|_{L^2}^2 \quad \text{and} \quad \mathcal{P}[\gamma] := \frac{1}{2} (\|\mathcal{I}[\gamma] - \mathcal{I}[\gamma_{\text{ref}}]\|_{L^2}^2 + \mu \|\gamma'\|_{L^2}^2),$$

and define the functional  $\mathcal{F}: L^2(\mathbb{S}^1, \mathbb{R}) \rightarrow \mathbb{R} \cup \{+\infty\}$  by

$$(3.3) \quad \mathcal{F}[\gamma] := \begin{cases} \sum_{i=1}^n \mathcal{D}_{\sigma_i}[\gamma] + \beta \mathcal{P}[\gamma] & \text{if } \gamma \in H^1(\mathbb{S}^1, \mathbb{R}_+), \\ +\infty & \text{else.} \end{cases}$$

The operator  $\mathcal{R}_{\sigma_i}$  is defined for a function depending on values on  $\mathbb{S}^1$ . Therefore, its evaluation at a specific point  $\alpha$  should be written as an integral over a subset of  $\mathbb{S}^1$  as well. A simple parameter transform yields the following reformulation of the operator.

**Lemma 3.5.** Let  $\sigma_i \in \mathbb{S}^1$ . Denote by  $H_1(x)$  the Heaviside function defined by  $H_1(x) = 0$  for  $x < 1$  and  $H_1(x) = 1$  for  $x \geq 1$ , and define the half-sphere

$$\mathbb{S}_{\sigma_i, \alpha}^1 := \{\tau \in \mathbb{S}^1 : \text{sign}(\langle \tau, \sigma_i^\perp \rangle) = \text{sign}(\alpha)\}.$$

The operator  $\mathcal{R}_{\sigma_i}$  of Definition 3.2 can be written as

$$(3.4) \quad \mathcal{R}_{\sigma_i}[\gamma](\alpha) = \begin{cases} \int_{\mathbb{S}_{\sigma_i, \alpha}^1} H_1\left(\frac{\gamma(\tau) \langle \tau, \sigma_i^\perp \rangle}{\alpha}\right) \frac{|\alpha|}{\langle \tau, \sigma_i^\perp \rangle^2} d\mathcal{H}^1(\tau), & \alpha \neq 0, \\ \gamma(\sigma_i) + \gamma(-\sigma_i), & \alpha = 0. \end{cases}$$

*Proof.* Let  $\alpha \in \mathbb{R} \setminus \{0\}$  and  $\sigma_i \in \mathbb{S}^1$  be fixed. Define  $f_{\sigma_i, \alpha}: \mathbb{S}_{\sigma_i, \alpha}^1 \rightarrow \mathbb{R}$  by

$$f_{\sigma_i, \alpha}(\tau) := \frac{\langle \tau, \sigma_i \rangle}{\langle \tau, \sigma_i^\perp \rangle} \alpha.$$

That is,  $f_{\sigma_i, \alpha}$  maps a direction  $\tau \in \mathbb{S}_{\sigma_i, \alpha}^1$  to the line parallel to  $\sigma_i$  with offset  $\alpha$  (see Figure 2). A short calculation shows that  $\|Df_{\sigma_i, \alpha}(\tau)\| = |\alpha|/\langle \tau, \sigma_i^\perp \rangle^2$ , and, as a consequence, we obtain

$$\begin{aligned} \int_{\mathbb{S}_{\sigma_i, \alpha}^1} H_1\left(\frac{\gamma(\tau)\langle \tau, \sigma_i^\perp \rangle}{\alpha}\right) \frac{|\alpha|}{\langle \tau, \sigma_i^\perp \rangle^2} d\mathcal{H}^1(\tau) \\ &= \int_{\mathbb{R}} \left( \int_{f_{\sigma_i, \alpha}^{-1}(t) \cap \mathbb{S}_{\sigma_i, \alpha}^1} H_1\left(\frac{\gamma(\tau)\langle \tau, \sigma_i^\perp \rangle}{\alpha}\right) d\mathcal{H}^0(\tau) \right) d\mathcal{H}^1(t) \\ &= \int_{\mathbb{R}} H_1\left(\frac{\gamma(f_{\sigma_i, \alpha}^{-1}(t))\langle f_{\sigma_i, \alpha}^{-1}(t), \sigma_i^\perp \rangle}{\alpha}\right) d\mathcal{L}^1(t). \end{aligned}$$

Thus, the assertion follows from the fact that (see Figure 2)

$$\{t \in \mathbb{R} : \gamma(f_{\sigma_i, \alpha}^{-1}(t))\langle f_{\sigma_i, \alpha}^{-1}(t), \sigma_i^\perp \rangle/\alpha \geq 1\} = \{t \in \mathbb{R} : \alpha\sigma_i^\perp + t\sigma_i \in \Omega_\gamma\}. \quad \blacksquare$$

The optimality condition for (3.3) involves the derivative of the functional  $\mathcal{R}_{\sigma_i}$ , which, however, is not differentiable, because the integrand is the shifted Heaviside function  $H_1$ . For the numerical implementation of the minimizing procedure we replace the original functional  $\mathcal{F}$  by a differentiable version  $\mathcal{F}_\varepsilon$  based on a smoothed approximation of  $\mathcal{R}_{\sigma_i}$ .

**Definition 3.6.** Let  $0 < \varepsilon < 1$  and  $\sigma_i \in \mathbb{S}^1$  be fixed. Define the operator  $\mathcal{R}_{\sigma_i, \varepsilon}: L^2(\mathbb{S}^1, \mathbb{R}_+) \rightarrow L^1(\mathbb{R}, \mathbb{R}_+)$  by

$$(3.5) \quad \mathcal{R}_{\sigma_i, \varepsilon}[\gamma](\alpha) := \begin{cases} \int_{\mathbb{S}_{\sigma_i, \alpha}^1} H_{1, \varepsilon}\left(\frac{\gamma(\tau)\langle \tau, \sigma_i^\perp \rangle}{\alpha}\right) \frac{|\alpha|}{\langle \tau, \sigma_i^\perp \rangle^2} d\mathcal{H}^1(\tau), & \alpha \neq 0, \\ \gamma(\sigma_i) + \gamma(-\sigma_i), & \alpha = 0. \end{cases}$$

Here,  $H_{1, \varepsilon}$  denotes the mollification of the shifted Heaviside function.

**Definition 3.7.** Let  $\beta, \mu > 0$  and  $\gamma_{\text{ref}} \in L^2(\mathbb{S}^1, \mathbb{R}_+)$ . In addition, denote by  $\mathcal{I}: L^2(\mathbb{S}^1, \mathbb{R}_+) \rightarrow L^2(\mathbb{S}^1, \mathbb{R}_+)$  the circular integral invariant defined by (2.4). For  $\sigma_i \in \mathbb{S}^1$ ,  $f_i \in L^2(\mathbb{R}, \mathbb{R})$ ,  $i = 1, \dots, n$ , and  $0 < \varepsilon < 1$  define

$$\mathcal{D}_{\sigma_i, \varepsilon}[\gamma] := \frac{1}{2} \|\mathcal{R}_{\sigma_i, \varepsilon}[\gamma] - f_i\|_{L^2}^2 \quad \text{and} \quad \mathcal{P}[\gamma] := \frac{1}{2} (\|\mathcal{I}[\gamma] - \mathcal{I}[\gamma_{\text{ref}}]\|_{L^2}^2 + \mu \|\gamma'\|_{L^2}^2),$$

and define the functional  $\mathcal{F}_\varepsilon: L^2(\mathbb{S}, \mathbb{R}) \rightarrow \mathbb{R} \cup \{+\infty\}$  by

$$(3.6) \quad \mathcal{F}_\varepsilon[\gamma] := \begin{cases} \sum_{i=1}^n \mathcal{D}_{\sigma_i, \varepsilon}[\gamma] + \beta \mathcal{P}[\gamma] & \text{if } \gamma \in H^1(\mathbb{S}^1, \mathbb{R}_+), \\ +\infty & \text{else.} \end{cases}$$



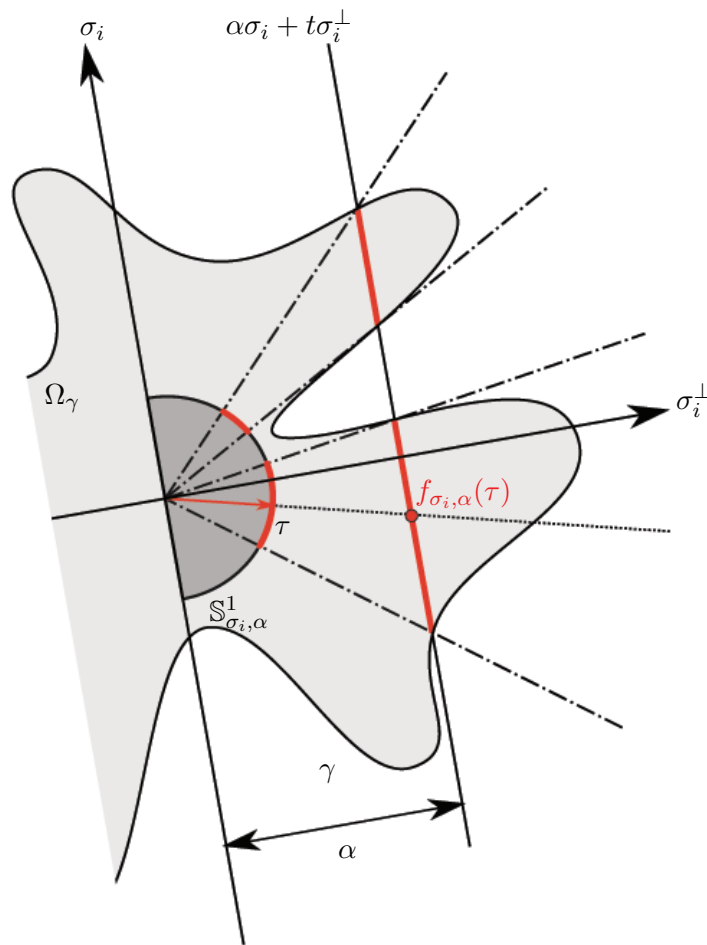


Figure 2. Sketch of the parameter transform  $f_{\sigma_i, \alpha}$ .

The existence of minimizers of the functional  $\mathcal{F}$  and its approximation  $\mathcal{F}_\varepsilon$  is guaranteed by the following theorem.

**Theorem 3.8.** *The functionals  $\mathcal{F}$  and  $\mathcal{F}_\varepsilon$  of Definitions 3.4 and 3.7 are lower semicontinuous and coercive.*

*Proof.* We show only the lower semicontinuity and the coercivity of  $\mathcal{F}_\varepsilon$ , the proof for  $\mathcal{F}$  being analogous.

Theorem 6.49 in [7] implies continuity of the mapping  $\gamma \mapsto \mathcal{R}_{\sigma_i, \varepsilon}[\gamma](\alpha)$  for every  $\alpha \in \mathbb{R}$ . As a consequence, applying Fatou's lemma, we obtain lower semicontinuity of  $\mathcal{R}_{\sigma_i, \varepsilon}$ . Proposition 10.7 in [23] shows lower semicontinuity of the smoothing term, and continuity of the integral invariant (see Theorem 2.4) in particular implies lower semicontinuity.

It remains to show that the functional  $\mathcal{F}_\varepsilon$  is coercive. To that end, we show in the following that every level set of  $\mathcal{F}_\varepsilon$  is bounded in  $H^1(\mathbb{S}^1, \mathbb{R})$  and, therefore, by the Rellich–Kondrašov theorem (see [23, p. 258]), precompact in  $L^2(\mathbb{S}^1, \mathbb{R})$ . Therefore let  $t > 1$  and  $\gamma \in L^2(\mathbb{S}^1, \mathbb{R})$  such that  $\mathcal{F}_\varepsilon[\gamma] \leq t$ . Then, in particular, we know that  $\gamma \in H^1(\mathbb{S}^1, \mathbb{R}) \subset W^{1,1}(\mathbb{S}^1, \mathbb{R})$ . By

Theorem 18.17 in [13] we obtain for  $\varphi_1, \varphi_2 \in [0, 2\pi[$

$$|\gamma(\varphi_1) - \gamma(\varphi_2)| \leq \left| \int_{\varphi_1}^{\varphi_2} \gamma'(\varphi) d\mathcal{L}^1(\varphi) \right| \leq \int_{\mathbb{S}^1} |\gamma'(\tau)| d\mathcal{H}^1(\tau) = \|\gamma'\|_{L^1(\mathbb{S}^1, \mathbb{R})}$$

and, in particular,

$$(3.7) \quad \left| \max_{\tau \in \mathbb{S}^1} \gamma(\tau) - \min_{\tau \in \mathbb{S}^1} \gamma(\tau) \right| \leq \|\gamma'\|_{L^1(\mathbb{S}^1, \mathbb{R})} \leq \sqrt{2\pi} \|\gamma'\|_{L^2(\mathbb{S}^1, \mathbb{R})} \leq 2\sqrt{\frac{\pi t}{\beta\mu}}.$$

Now let  $1 \leq i \leq n$  be fixed. Because  $f_i \in L^2(\mathbb{R}, \mathbb{R})$ , there exists some  $\tilde{r} > 0$  such that

$$(3.8) \quad \left( \int_{|x| > \tilde{r}} f_i^2(x) d\mathcal{L}^1(x) \right)^{1/2} < \sqrt{2} - 1.$$

Let  $r := \max\{\tilde{r}, \sqrt{t}\}$ . Now we show that

$$(3.9) \quad \min_{\tau \in \mathbb{S}^1} \gamma(\tau) \leq (2r + 1)(1 + \varepsilon) \quad \text{and} \quad \max_{\tau \in \mathbb{S}^1} \gamma(\tau) \leq (2r + 1)(1 + \varepsilon) + 2\sqrt{\frac{\pi t}{\beta\mu}}.$$

Assume to the contrary that

$$(3.10) \quad \min\{\gamma(\tau) : \tau \in \mathbb{S}^1\} > (2r + 1)(1 + \varepsilon).$$

Observe that for  $0 < \varepsilon < 1$  we have

$$H_1\left(\frac{t}{1 + \varepsilon}\right) \leq H_{1, \varepsilon}(t) \quad \text{and thus} \quad |\mathcal{R}_{\sigma_i, \varepsilon}[\gamma](\alpha)| \geq \left| \mathcal{R}_{\sigma_i} \left[ \frac{\gamma}{1 + \varepsilon} \right](\alpha) \right|.$$

A simple geometrical argument (see Figure 3) shows that

$$(3.11) \quad \left| \mathcal{R}_{\sigma_i} \left[ \frac{\gamma}{1 + \varepsilon} \right](\alpha) \right| \geq 2r \quad \text{for} \quad r < \alpha < r + 1.$$

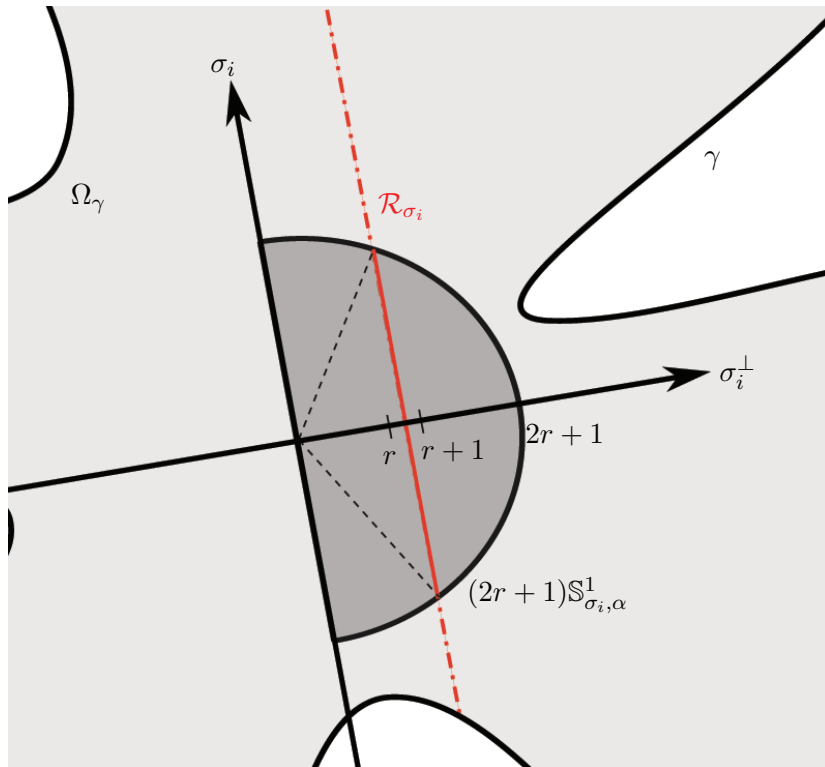
Define  $A := (r, r + 1)$ . Because  $t > 1$ , and by (3.8) and (3.11), it follows that

$$\begin{aligned} \sqrt{t} &\geq \|\mathcal{R}_{\sigma_i, \varepsilon}[\gamma] - f_i\|_{L^2(\mathbb{R})} \geq \|\mathcal{R}_{\sigma_i, \varepsilon}[\gamma] - f_i\|_{L^2(A)} \geq \|\mathcal{R}_{\sigma_i, \varepsilon}[\gamma]\|_{L^2(A)} - \|f_i\|_{L^2(A)} \\ &= \left( \int_A |\mathcal{R}_{\sigma_i, \varepsilon}[\gamma](\alpha)|^2 d\mathcal{L}^1(\alpha) \right)^{1/2} - \|f_i\|_{L^2(A)} > 2r - (\sqrt{2} - 1) \\ &> 2\sqrt{t} - (\sqrt{2} - 1)\sqrt{t} > \sqrt{t}, \end{aligned}$$

which yields a contradiction to (3.10). Thus the first inequality in (3.9) holds. The second inequality is now a consequence of (3.7). Therefore, we can bound the  $L^2$ -norm of  $\gamma$  by

$$(3.12) \quad \|\gamma\|_{L^2(\mathbb{S}^1, \mathbb{R})}^2 \leq 2\pi \left( \max_{\tau \in \mathbb{S}^1} \gamma(\tau) \right)^2 \leq 2\pi \left( (2 \max\{\tilde{r}, \sqrt{t}\} + 1)(1 + \varepsilon) + 2\sqrt{\frac{\pi t}{\beta\mu}} \right)^2.$$

Together with (3.7), this shows that the level set of  $\mathcal{F}_\varepsilon$  to the level  $t$  is bounded in  $H^1(\mathbb{S}^1, \mathbb{R})$ . Application of the Rellich–Kondrašov theorem concludes the proof. ■



**Figure 3.** Sketch of the estimation of  $\mathcal{R}_{\sigma_i}[\frac{\gamma}{1+\varepsilon}]$  in (3.11).

**3.2.  $\Gamma$ -convergence.** In this section we show that the functional  $\mathcal{F}_\varepsilon$  is indeed an approximation of the original functional  $\mathcal{F}$ .

**Lemma 3.9.** *Let  $(\varepsilon_k) \rightarrow 0$ , and denote by  $(\gamma_{\varepsilon_k})$  a minimizing sequence of the functionals  $\mathcal{F}_{\varepsilon_k}$ . Then  $(\gamma_{\varepsilon_k})$  has a convergent subsequence in  $L^2(\mathbb{S}^1, \mathbb{R})$  and the limit of every convergent subsequence is a minimizer of  $\mathcal{F}$ .*

*Proof.* The basic idea is to prove  $\Gamma$ -convergence and equicoercivity of the approximating functionals  $\mathcal{F}_{\varepsilon_k}$ . First notice that equicoercivity is a direct consequence of (3.7) and (3.12) in the proof of Theorem 3.8.

In order to show  $\Gamma$ -convergence we have to verify the following two conditions (see [3, Chap. 8]):

1. For every  $\eta \in H^1(\mathbb{S}^1, \mathbb{R})$  and every sequence  $(\eta_k)$  in  $H^1(\mathbb{S}^1, \mathbb{R})$  converging to  $\eta$  with respect to the  $L^2$ -norm we have

$$(3.13) \quad \mathcal{F}[\eta] \leq \liminf_{k \rightarrow \infty} \mathcal{F}_{\varepsilon_k}[\eta_k].$$

2. For every  $\eta \in H^1(\mathbb{S}^1, \mathbb{R})$  there exists a sequence  $(\eta_k)$  in  $H^1(\mathbb{S}^1, \mathbb{R})$  converging to  $\eta$  with respect to the  $L^2$ -norm such that

$$\mathcal{F}[\eta] = \lim_{k \rightarrow \infty} \mathcal{F}_{\varepsilon_k}[\eta_k].$$

The latter condition follows immediately from the fact that  $\mathcal{F}_{\varepsilon_k}[\eta]$  converges to  $\mathcal{F}[\eta]$  as  $k \rightarrow \infty$  for every  $\eta \in L^2(\mathbb{S}^1, \mathbb{R})$ .

Let  $\eta \in H^1(\mathbb{S}^1, \mathbb{R})$ , and let  $(\eta_k)$  be any sequence in  $H^1(\mathbb{S}^1, \mathbb{R})$  converging to  $\eta$  with respect to the  $L^2$ -norm. We have to verify (3.13). Since the regularization term does not depend on  $\varepsilon_k$ , this is equivalent to showing that  $\mathcal{D}_{\sigma_i}[\eta] \leq \liminf_{k \rightarrow \infty} \mathcal{D}_{\sigma_i, \varepsilon_k}[\eta_k]$  for each direction  $\sigma_i \in \mathbb{S}^1$ . The continuity of  $\mathcal{R}_{\sigma_i}$  implies that, after possible passing to an appropriate subsequence,  $\mathcal{R}_k^\pm(\alpha) := \mathcal{R}_{\sigma_i}[\eta_k / (1 \pm \varepsilon_k)](\alpha) \rightarrow \mathcal{R}_{\sigma_i}[\eta](\alpha)$  pointwise almost everywhere. As a consequence, applying Fatou's lemma we obtain

$$\begin{aligned} \liminf_{k \rightarrow \infty} \mathcal{D}_{\sigma_i, \varepsilon_k}[\eta_k] &= \liminf_{k \rightarrow \infty} \int_{\mathbb{R}} |\mathcal{R}_{\sigma_i, \varepsilon_k}[\eta_k](\alpha) - f(\alpha)|^2 d\mathcal{L}^1(\alpha) \\ &\geq \int_{\mathbb{R}} \liminf_{k \rightarrow \infty} |\mathcal{R}_{\sigma_i, \varepsilon_k}[\eta_k](\alpha) - f(\alpha)|^2 d\mathcal{L}^1(\alpha) \\ &\geq \int_{\mathbb{R}} \liminf_{k \rightarrow \infty} \left( \min\{ |(\mathcal{R}_k^+ - f)(\alpha)|, |(\mathcal{R}_k^- - f)(\alpha)| \}^2 \right) d\mathcal{L}^1(\alpha) \\ &\quad - \int_{\mathbb{R}} \limsup_{k \rightarrow \infty} \left( |(\mathcal{R}_k^+ - \mathcal{R}_k^-)(\alpha)|^2 \right) d\mathcal{L}^1(\alpha) \\ &= \int_{\mathbb{R}} |\mathcal{R}_{\sigma_i}[\eta](\alpha) - f(\alpha)|^2 d\mathcal{L}^1(\alpha) \\ &= \mathcal{D}_{\sigma_i}[\eta], \end{aligned}$$

which proves the assertion.  $\blacksquare$

**4. Numerical results.** The actual optimization was performed with a gradient descent approach, which involves the derivative of the functional to minimize. Therefore we have based the numerical implementation on the smooth approximation functional  $\mathcal{F}_\varepsilon$ . The  $\Gamma$ -convergence of this functional to the original functional  $\mathcal{F}$ , shown in the previous section, implies that for a sufficiently small value of the smoothing parameter  $\varepsilon$  we obtain a solution that is close to an actual minimizer of  $\mathcal{F}$ . We have used a finite element approach with piecewise linear basis functions for the discretization of the regularization functional. All the integrations were realized by the trapezoidal rule. The iteration was stopped as soon as the maximal absolute value of the gradient of  $\mathcal{F}_\varepsilon$  was below some a priori chosen threshold.

For comparison, we have also implemented a Landweber–Kaczmarz method (see [16]) for the solution of (3.1), where the radial function of the prior was used as the initial value. This method aims to find an approximate solution that is close to the given prior by alternately taking steepest descent steps for the squared residuals  $\|\mathcal{R}_{\sigma_i, \varepsilon} - f_i\|^2$ , starting from the prior  $\gamma_{\text{ref}}$ . The iteration then reads as

$$\begin{aligned} \gamma_0 &= \gamma_{\text{ref}}, \\ \gamma_{k+1} &= \gamma_k + \lambda (D\mathcal{R}_{\sigma_{k \bmod n}, \varepsilon})^* (\mathcal{R}_{\sigma_{k \bmod n}, \varepsilon}[\gamma_k] - f_{k \bmod n}), \end{aligned}$$

where  $n$  denotes the number of directions in which the Radon transform is given. In order to obtain a regularization method, this iteration is stopped well before convergence is reached. The number and size of the steps taken determine the amount of regularization, fewer and

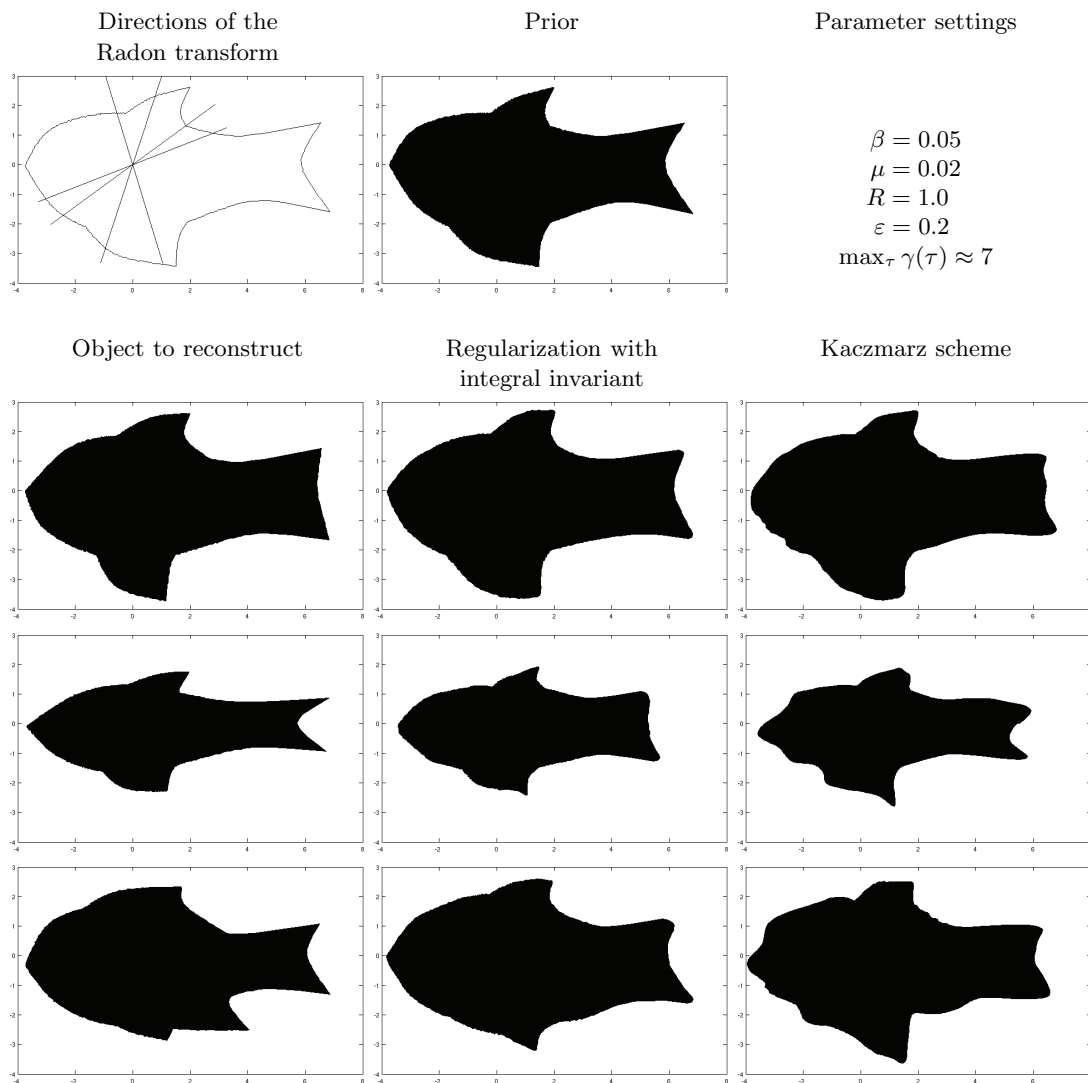
smaller steps leading to a result that is closer to the prior. In contrast to Tikhonov regularization with the functional  $\mathcal{F}_\varepsilon$ , where closeness of the prior in terms of the integral invariant is required, here the closeness of the radial functions themselves is measured. In order to avoid spurious oscillations in the result we have in addition added a smoothing term in each iteration step. Also, with this regularization the two methods are more comparable. The regularized iteration then reads as

$$(4.1) \quad \gamma_{k+1} = \gamma_k + \lambda \left[ (D\mathcal{R}_{\sigma_k \bmod n, \varepsilon})^* (\mathcal{R}_{\sigma_k \bmod n, \varepsilon}[\gamma_k] - f_{k \bmod n}) - \mu \gamma_k'' \right].$$

Notice that for the following numerical examples the constant  $\mu$  was chosen much smaller than 1. Moreover, we have used the same constant  $\mu$  for the regularization method given in Definition 3.7.

In all the numerical examples we have tried to reconstruct an object from its Radon transform given only in four directions. This data would allow a unique reconstruction if we restricted the set of solutions to convex objects [9, Corollary 1.2.12]. In the case of a star-shaped body, however, the same data is insufficient for a successful reconstruction [9, Theorem 2.3.4] and, consequently, the problem is ill-posed. To amplify the effect of ill-posedness we have chosen the four directions in such a way that significant parts of the object are only poorly resolved (cf. Figures 4 and 5, upper left, where  $\sigma_i \in \{21.6^\circ, 36^\circ, 72^\circ, 108^\circ\}$ ). For the numerical experiments we fixed the reference object (see Figures 4 and 5, first row) and used visually similar objects to compute artificial data sets for  $\mathcal{R}_{\sigma_i, \varepsilon}$  for  $i = 1, \dots, 4$  and  $\varepsilon < 1$ . The results of the reconstruction with Tikhonov regularization using the integral invariant in the prior term are depicted in Figures 4 and 5, middle column; the results of the reconstruction with the Landweber–Kaczmarz scheme (4.1) are depicted in Figures 4 and 5, right column. In both figures the left column shows the object from which the data is computed, which at the same time is the object to be reconstructed.

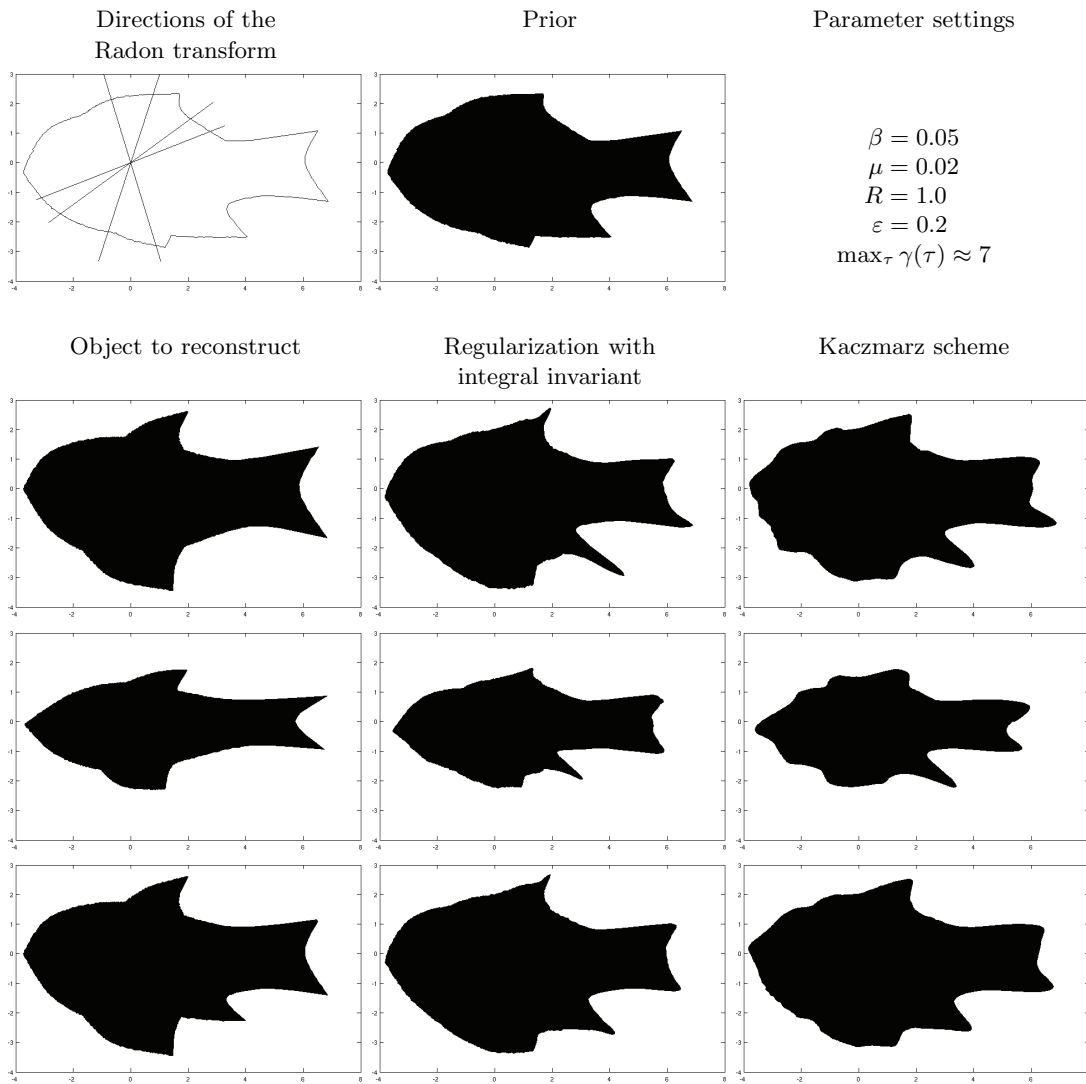
As can be seen from the figures, the Landweber–Kaczmarz scheme produces artefacts in regions where the features of the object are poorly resolved by the Radon transform. This is quite natural, as in (4.1) only the data is used and the prior knowledge about the geometry of the object is solely incorporated as the initial value of the iteration. In contrast, because in the poorly resolved regions of the object the integral invariant of the prior covers the geometry, our method is capable of handling this lack of information and produces reconstructions that are visually more appealing. These differences can be seen best in Figure 4, last two rows: Compare, in particular, the shape of the fish head. Admittedly, artefacts are also present in our results, but they are limited to parts of the object where the prior information contradicts the object we want to reconstruct. Thus, the artefacts are rather due to wrong a priori knowledge than to a failure of the method. This effect occurs, for instance, in the first two reconstructions in Figure 5, especially at the second lower fin, which is present in the prior but missing in the objects of interest. Thus, both the regularization method and the Landweber–Kaczmarz scheme try to reconstruct a feature that does not exist. Again, we want to emphasize that our method does not introduce additional artefacts in parts where the prior information is consistent with the true solution, whereas the Landweber–Kaczmarz scheme does, which is a significant advantage of our approach. In addition, the numerical results indicate that our method is well capable of handling scaled objects (see Figure 4, middle row), which is a



**Figure 4.** Reconstruction with fixed reference object (prior) shown in the first row. First column: object to reconstruct. Second column: reconstruction based on regularization with the circular integral invariant. Third column: reconstruction based on the Landweber–Kaczmarz scheme.

consequence of the fact that the integral invariant reflects mainly curvature information of the prior [22].

*Remark 4.1.* As was mentioned at the beginning of section 3.1 one would also have to incorporate the influence of the two parameters introduced by the parametrization via a radial function (center of star-shapedness and angle of rotation). In the case of the prior one can follow the approach given in Remark 2.5 for choosing the center of star-shapedness and realignment of the radial function. For the reconstruction of a given data set it is then necessary to ensure that the underlying unknown object is aligned in the same way. Because we are given the Radon transform only in four directions, the alignment of the object cannot



**Figure 5.** Reconstruction with fixed reference object (prior) shown in the first row. First column: object to reconstruct. Second column: reconstruction based on regularization with the circular integral invariant. Third column: reconstruction based on the Landweber–Kaczmarz scheme.

be estimated directly from the data. The approach to bypassing this problem that we have used in our implementation is to compute the best possible match of the Radon transform of the prior and the given data and use the result for the alignment of the initial value of the iteration. In addition, one can realign the object during the iteration, again by matching the Radon transform of the current iterate with the data.

**5. Conclusion.** In this article we have introduced a Tikhonov-like regularization functional for the reconstruction of star-shaped objects, which is based on the difference of integral invariants. As a case example, we have considered the problem of reconstructing an object from its Radon transform given only for a finite number of directions. We have derived the

necessary theoretical background to show existence of minimizers of the Tikhonov functional and introduced a smooth approximation used for numerical computations. The presented numerical results indicate that the approach based on integral invariants is suitable for the estimation of objects in case of insufficient data. In particular, the comparison with a standard iterative approach has shown that our method creates significantly fewer artefacts.

**Appendix.** In this section we present some additional numerical results in order to demonstrate the performance of the proposed regularization strategy based on the difference of integral invariants and also to show the necessity of regularization. To that end, we have performed a series of experiments, where we have generated artificial data from a number of test images, and have applied our proposed method for varying priors both in the noise-free case and also in the presence of noise.

The following tables contain several key values of the reconstruction process, namely the data fidelity term (the squared  $L^2$ -distance of the data and the regularized Radon transform of the reconstruction) as well as the distance between the reconstructed shape and, first, the true solution (the shape from which the data was generated) and, second, the shape that was used as the prior in the specific experiment. All the shape distances are given in terms of the squared  $L^2$ -norm of the difference of the radial functions.

Table 1 shows the numerical results in the absence of noise. In this case, the reconstruction works well independent of the regularization parameter (the parameter in the table was chosen to be small in order to highlight this independence). Note that the true solutions are not recovered exactly because of the presence of the additional regularization term penalizing the norm of the derivative of the radial functions. If, however, the data set is affected by noise, the quality of the results deteriorates drastically. In Tables 2 and 3, the results for the same combination of data sets and priors are shown as in Table 1 but now in the case of noisy data with a noise level of about 15%. One can see that the distance between the reconstructions and the true solutions is much larger than in the noise-free case. In addition, one can see the beneficial effect of regularization: In Table 2, we chose a small regularization parameter, while in Table 3 the regularization parameter was chosen quite large. Accordingly, the method provides better results in the latter situation than in the former one. However, one also sees that the results become better, even if one chooses a wrong prior, as long as some features of the true solution are also present in the prior. Such a behavior would not be possible if the regularization were based on the  $L^2$ -distance of the radial functions themselves and not on the distance between their integral invariants.



Table 1

Reconstruction with unperturbed data and weak regularization:  $\beta = 0.1$ ,  $\mu = 0.02$ ,  $R = 1.0$ ,  $\varepsilon = 0.2$ . The displayed values show the squared  $L^2$ -distances of the data and the Radon transform of the reconstruction (top), the radial function of the reconstruction and of the true solution (middle), and the radial function of the reconstruction and of the prior (bottom). The values in boldface show the minima in each line.









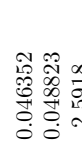
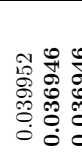
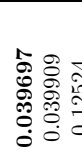
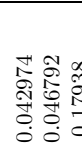
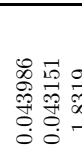










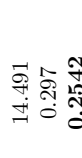
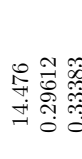

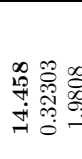
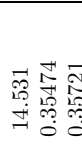








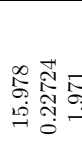
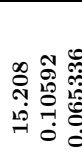
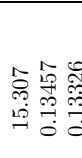
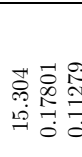
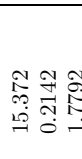
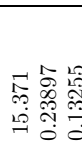
Prior							
Goal							
	0.046352 0.048823 2.5918	0.039952 <b>0.036946</b> <b>0.036946</b>	0.034564 0.031087 0.11988	0.035295 0.035521 0.16922	0.042974 0.046792 0.17938	0.043986 0.043151 1.8319	0.044887 0.048298 0.20904
	0.037871 0.038916 2.6486	0.034564 0.031087 0.11988	<b>0.033214</b> <b>0.028253</b> <b>0.028253</b>	0.035295 0.035521 0.16922	0.035295 0.035521 0.16922	0.03641 0.035241 2.3283	0.038321 0.04027 0.29016
	0.034587 0.025997 2.2018	0.033374 0.02353 0.2319	0.032406 0.023119 0.21516	<b>0.032114</b> <b>0.02297</b> <b>0.02297</b>	<b>0.032114</b> <b>0.02297</b> <b>0.02297</b>	0.033997 0.027846 2.4612	0.033894 0.024944 0.71288
	0.040966 0.035709 3.755	0.03718 0.031381 1.9293	0.039006 0.035341 2.4311	0.038786 0.034464 2.382	0.038786 0.034464 2.382	<b>0.032184</b> <b>0.028354</b> <b>0.028354</b>	0.036527 0.030401 1.9201
	0.032232 0.027332 2.5157	0.029325 0.024712 0.26806	0.029504 0.025879 0.34139	0.031176 0.026118 0.3116	0.031499 0.025499 2.1323	0.031499 0.025499 2.1323	0.028236 0.026153 0.33737
	0.04208 0.037138 2.143	0.042208 0.034146 0.70364	0.041787 0.0341 0.8514	0.041238 0.035581 0.74648	0.04235 0.035464 2.008	0.040106 0.034768 0.31978	<b>0.039168</b> <b>0.03387</b> <b>0.03387</b>

Table 2

Reconstruction with noisy data and weak regularization:  $\beta = 0.1$ ,  $\mu = 0.02$ ,  $R = 1.0$ ,  $\varepsilon = 0.2$ , noise level = 15%. The displayed values show the squared  $L^2$ -distances of the data and the Radon transform of the reconstruction (top), the radial function of the reconstruction and of the true solution (middle), and the radial function of the reconstruction and of the prior (bottom). The values in boldface show the minima in each line.

Prior							
Goal							
	14.986 0.30523 2.228	14.491 0.297 <b>0.2542</b>	14.476 0.29612 0.33383	14.512 <b>0.2833</b> 0.26339	14.458 0.32303 1.9808	14.531 0.35474 0.35721	14.57 0.42395 0.6184
	14.932 0.33685 2.3189	14.4 <b>0.29808</b> 0.34557	14.378 0.30075 <b>0.26411</b>	14.366 0.31009 0.29336	14.372 0.32094 2.4113	14.434 0.49516 0.34405	14.451 0.56369 0.65453
	14.98 0.32142 1.9144	14.524 0.28489 0.52334	14.511 0.28577 0.48728	14.513 0.27897 <b>0.23526</b>	14.519 <b>0.27029</b> 2.6551	14.437 0.38668 0.68975	<b>14.429</b> 0.39291 1.0144
	15.538 0.27394 3.5904	14.966 <b>0.17052</b> 1.9756	14.948 0.20866 2.6524	14.919 0.20137 2.6318	14.575 0.19892 <b>0.16853</b>	14.837 0.19463 2.3616	14.831 0.20256 2.0635
	14.933 0.36815 2.1476	14.425 0.33741 0.38265	14.417 0.34529 0.46192	14.327 0.39683 0.42373	14.362 0.33085 2.1162	14.352 <b>0.28467</b> <b>0.24168</b>	14.331 0.31945 0.51791
	15.059 0.31112 1.7105	14.563 0.35295 0.84595	14.513 0.37169 1.0225	14.487 0.38039 0.82222	14.488 0.32829 2.0766	14.429 0.33415 0.5641	14.484 <b>0.2797</b> <b>0.22809</b>

**Table 3**  
*Reconstruction with noisy data and strong regularization:  $\beta = 10$ ,  $\mu = 0.0002$ ,  $R = 1.0$ ,  $\varepsilon = 0.2$ , noise level = 15%. The displayed values show the squared  $L^2$ -distances of the data and the Radon transform of the reconstruction (top), the radial function of the reconstruction and of the true solution (middle), and the radial function of the reconstruction and of the prior (bottom). The values in boldface show the minima in each line.*

Prior							
Goal							
	15.978 0.22724 1.971	<b>15.208</b> <b>0.10592</b> <b>0.065336</b>	15.307 0.13457 0.13326	15.304 0.17801 0.11279	15.372 0.2142 1.7792	15.371 0.23897 0.13255	15.394 0.40387 0.39508
	15.821 0.26077 1.9965	15.196 0.10623 0.13418	15.162 <b>0.10414</b> <b>0.067912</b>	15.171 0.15366 0.1184	15.299 0.22394 2.2044	15.247 0.3662 0.13745	<b>15.159</b> 0.47265 0.46882
	15.855 0.22773 1.6023	15.385 0.10687 0.27795	15.33 <b>0.085394</b> 0.26069	<b>15.24</b> 0.1063 <b>0.06272</b>	15.359 0.20108 2.4705	15.533 0.245 0.26045	15.404 0.33334 0.54266
	16.269 0.21844 3.1649	16.07 0.15036 1.6816	16.096 0.18815 2.224	15.924 0.19243 2.2626	<b>15.025</b> <b>0.059803</b> <b>0.031519</b>	16.216 0.36739 1.8569	15.97 0.27766 1.7173
	16.139 0.26726 1.9041	15.384 0.19795 0.11157	15.485 0.21502 0.1418	15.455 0.19396 0.1189	15.341 0.21704 1.9017	<b>15.13</b> <b>0.07716</b> <b>0.045982</b>	15.229 0.12742 0.27495
	15.944 0.21928 1.4584	15.648 0.2965 0.40657	15.641 0.30492 0.5018	15.514 0.26851 0.4236	15.438 0.24268 1.8045	15.322 0.15479 0.28915	<b>15.119</b> <b>0.12071</b> <b>0.072868</b>

## REFERENCES

- [1] M. BAUER, T. FIDLER, AND M. GRASMAIR, *Local Uniqueness of the Circular Integral Invariant*, <http://arxiv.org/abs/1107.4257> (2011).
- [2] E. CALABI, P. J. OLVER, C. SHAKIBAN, A. TANNENBAUM, AND S. HAKER, *Differential and numerically invariant signature curves applied to object recognition*, *Int. J. Comput. Vis.*, 26 (1998), pp. 107–135.
- [3] G. DAL MASO, *An Introduction to  $\Gamma$ -Convergence*, *Progr. Nonlinear Differential Equations Appl.* 8, Birkhäuser, Boston, 1993.
- [4] T. FIDLER, M. GRASMAIR, H. POTTMANN, AND O. SCHERZER, *Inverse Problems of Integral Invariants and Shape Signatures*, Reports of FSP S092 - “Industrial Geometry” 40, University of Innsbruck, Innsbruck, Austria, 2007.
- [5] T. FIDLER, M. GRASMAIR, AND O. SCHERZER, *Identifiability and reconstruction of shapes from integral invariants*, *Inverse Probl. Imaging*, 2 (2008), pp. 341–354.
- [6] P. T. FLETCHER, C. LU, S. M. PIZER, AND S. JOSHI, *Principal geodesic analysis for the study of nonlinear statistics of shape*, *IEEE Trans. Med. Imag.*, 23 (2004), pp. 995–1005.
- [7] I. FONSECA AND G. LEONI, *Modern Methods in the Calculus of Variations:  $L^p$  Spaces*, Springer Monogr. Math., Springer, New York, 2007.
- [8] M. FUCHS AND O. SCHERZER, *Regularized reconstruction of shapes with statistical a priori knowledge*, *Int. J. Comput. Vis.*, 79 (2008), pp. 119–135.
- [9] R. J. GARDNER, *Geometric Tomography*, 2nd ed., *Encyclopedia Math. Appl.* 58, Cambridge University Press, Cambridge, UK, 2006.
- [10] F. HETTLICH AND W. RUNDELL, *Iterative methods for the reconstruction of an inverse potential problem*, *Inverse Problems*, 12 (1996), pp. 251–266.
- [11] F. HETTLICH AND W. RUNDELL, *The determination of a discontinuity in a conductivity from a single boundary measurement*, *Inverse Problems*, 14 (1998), pp. 67–82.
- [12] F. HETTLICH AND W. RUNDELL, *Identification of a discontinuous source in the heat equation*, *Inverse Problems*, 17 (2001), pp. 1465–1482.
- [13] E. HEWITT AND K. STROMBERG, *Real and Abstract Analysis*, Springer, New York, 1965.
- [14] Q.-X. HUANG, S. FLÖRY, N. GELFAND, M. HOFER, AND H. POTTMANN, *Reassembling fractured objects by geometric matching*, *ACM Trans. Graph.*, 25 (2006), pp. 569–578.
- [15] D. HULIN AND M. TROYANOV, *Mean curvature and asymptotic volume of small balls*, *Amer. Math. Monthly*, 110 (2003), pp. 947–950.
- [16] B. KALTENBACHER, A. NEUBAUER, AND O. SCHERZER, *Iterative Regularization Methods for Nonlinear Ill-Posed Problems*, *Radon Ser. Comput. Appl. Math.* 6, Walter de Gruyter, Berlin, 2008.
- [17] D. G. KENDALL, *Shape manifolds, procrustean metrics and complex projective spaces*, *Bull. London Math. Soc.*, 16 (1984), pp. 81–121.
- [18] H. KRIM AND A. J. YEZZI, JR., *Statistics and Analysis of Shapes*, Birkhäuser, Boston, 2006.
- [19] S. MANAY, D. CREMERS, B.-W. HONG, A. J. YEZZI, JR., AND S. SOATTO, *Integral invariants and shape matching*, in *Statistics and Analysis of Shapes*, Birkhäuser, Boston, 2006, pp. 137–166.
- [20] S. MANAY, D. CREMERS, A. J. YEZZI, JR., AND S. SOATTO, *One-shot integral invariant shape priors for variational segmentation*, in *Energy Minimization Methods in Computer Vision and Pattern Recognition*, *Lecture Notes in Comput. Sci.* 3757, A. Rangarajan, B. Vemuri, and A. Yuille, eds., Springer, Berlin, Heidelberg, 2005, pp. 414–426.
- [21] P. W. MICHOR AND D. MUMFORD, *Riemannian geometries on spaces of plane curves*, *J. Eur. Math. Soc. (JEMS)*, 8 (2006), pp. 1–48.
- [22] H. POTTMANN, J. WALLNER, Q.-X. HUANG, AND Y.-L. YANG, *Integral invariants for robust geometry processing*, *Comput. Aided Geom. Design*, 26 (2009), pp. 37–60.
- [23] O. SCHERZER, M. GRASMAIR, H. GROSSAUER, M. HALTMEIER, AND F. LENZEN, *Variational Methods in Imaging*, *Appl. Math. Sci.* 167, Springer, New York, 2009.
- [24] R. T. WHITAKER AND V. ELANGOVAN, *A direct approach to estimating surfaces in tomographic data*, *Med. Image Anal.*, 6 (2002), pp. 235–249.
- [25] P. YUSHKEVICH, P. T. FLETCHER, S. JOSHI, A. THALL, AND S. M. PIZER, *Continuous medial representations for geometric object modeling in 2D and 3D*, *Image Vis. Comput.*, 21 (2003), pp. 17–27.